

Testing the space-time geometry around black hole candidates with the available radio and X-ray data

Cosimo Bambi

*Center for Field Theory and Particle Physics & Department of Physics,
Fudan University, 200433 Shanghai, China*

bambi@fudan.edu.cn

August 30, 2018

ABSTRACT

Astrophysical black hole candidates are thought to be the Kerr black holes predicted by General Relativity, but the actual nature of these objects has still to be proven. The Kerr black hole hypothesis can be tested by observing strong gravity features and check if they are in agreement with the predictions of General Relativity. In particular, the study of the properties of the electromagnetic radiation emitted by the gas of the accretion disk can provide information on the geometry of the space-time around these objects and constrain possible deviations from the Kerr background.

Subject headings: black hole physics — general relativity — accretion, accretion disks

1. Introduction

The predictions of General Relativity have been confirmed by experiments in the Earth's gravitational field (Williams et al. 2004; Everitt et al. 2011), by spacecraft missions in the Solar System (Bertotti et al. 2003), and by accurate radio observations of binary pulsars (Weisberg & Taylor 2005; Kramer et al. 2006) (for a general review, see e.g. Will (2006)). In all these environments, the gravitational field is weak, in the sense that one can write $g_{tt} = 1 + \phi$ with $|\phi| \ll 1$. The validity of the theory in the regime of strong gravity, when the approximation $|\phi| \ll 1$ breaks down, is instead still unexplored. The ideal laboratory to test strong gravitational fields is the space-time around astrophysical black hole (BH) candidates.

In 4-dimensional General Relativity, uncharged BHs are described by the Kerr solution and are completely specified by two parameters: the mass, M , and the spin angular momentum, J (Carter 1971; Robinson 1975)¹. A fundamental limit for a Kerr BH is the bound $|a_*| \leq 1$, where $a_* = J/M^2$ is the spin parameter. This is the condition for the existence of the event horizon: for $|a_*| > 1$, the event horizon disappears, and the central singularity becomes naked, violating the weak cosmic censorship conjecture (Penrose 1969). Despite the apparent possibility of forming naked singularities from regular initial data (see e.g. Joshi & Malafarina (2011a,b) and references therein), the existence of a Kerr naked singularity or of a super-spinning Kerr compact object (in which the singularity may be replaced by an extremely compact object made of exotic matter) can be excluded for at least two reasons: it is apparently impossible to make a star collapse with $|a_*| > 1$ (Giacomazzo et al. 2011) or overspin an already existing Kerr BH up to $|a_*| > 1$ (Barausse et al. 2010, 2011), and, even if created, this super-spinning object would be unstable and should quickly decay (Dotti et al. 2008; Pani et al. 2010).

Astrophysical BHs presumably form from the gravitational collapse of matter, while the BH uniqueness theorems require a stationary space-time. However, initial deviations from the Kerr solution should be quickly radiated away through the emission of gravitational waves (Price 1972a,b) (but see Lyutikov & McKinney (2011)), and the geometry of the space-time around the compact object should be well described by the Kerr metric². At the moment, there are at least two classes of astrophysical BH candidates (for a review, see e.g. Narayan (2005)): stellar-mass compact objects in X-ray binary systems ($M \approx 5 - 20 M_\odot$), and super-massive bodies at the center of every normal galaxy ($M \sim 10^5 - 10^9 M_\odot$). The measurement of the mass of the two classes of BH candidates is robust, because obtained by dynamical methods and without any assumption about the nature of these objects: basically, we can study the orbital motion of gas or of individual stars orbiting around the compact object and we can infer the mass of the latter by using Newtonian mechanics. Stellar-mass BH candidates are too heavy to be neutron or quark stars (Rhoades & Ruffini 1974; Kalogera & Baym 1996), while at least some of the super-massive objects in galactic nuclei are too heavy, compact, and old to be clusters of non-luminous bodies (Maoz 1998). The non-observation of electromagnetic radiation emitted by the possible surface of these objects may also be

¹The Kerr metric is a vacuum exact solution even in other theories of gravity, but its uniqueness is not guaranteed in general (Psaltis et al. 2008). The scenario of Kerr BHs in an alternative theory of gravity may be tested by looking for observational features that do not depend only on the metric of the background, such as the quasi-normal modes of the compact object (Barausse & Sotiriou 2008).

²Deviations from the Kerr metric due to the presence of an accretion disk should also be extremely small in the case of a compact object in an X-ray binary system. However, the presence of surrounding material might be important for some super-massive compact objects in galactic nuclei.

interpreted as an indications that they have an event horizon and are therefore BHs (Narayan & Heyl 2002; McClintock et al. 2004; Narayan & McClintock 2008; Broderick et al. 2009) (see however Abramowicz et al. (2002) and Bambi (2012e)). As there is no alternative explanation in the framework of conventional physics, astrophysical BH candidates are thought to be the Kerr BHs predicted by General Relativity, even if we have no evidence that the geometry of the space-time around them is really described by the Kerr solution.

The first proposal for testing the Kerr BH hypothesis was put forward by Ryan, who suggested to observe the gravitational waves emitted by an extreme-mass ratio inspiral (EMRI), i.e. a system consisting of a stellar-mass compact object orbiting around a super-massive BH candidate (Ryan 1995): as future space-based gravitational wave detectors will be able to observe $\sim 10^4 - 10^6$ gravitational wave cycles emitted by an EMRI while the stellar-mass body is inspiraling into the gravitational field of the super-massive object, even a small deviation from the Kerr geometry will build up an observable dephasing in the gravitational waveforms, thus allowing one to map the space-time of the super-massive BH candidate with very high accuracy (Glampedakis & Babak 2006; Barack & Cutler 2007). Besides tests based on gravitational waves, the space-time geometry around BH candidates can be probed by very accurate observations of the orbital motion of stars. In the case of a stellar-mass BH candidate in an X-ray binary system, that is possible if the companion star is a radio pulsar (Wex & Kopeikin 1999). In the case of the super-massive BH candidate at the center of our Galaxy, that might be achieved by monitoring stars orbiting at milliparsec distances from the compact object (Will 2008).

Recently, there has been an increasing new interest in the subject. While previous studies focused on future facilities (like space-based gravitational wave detectors) or possible future discoveries (like a BH binary with a pulsar companion), more recent efforts deal with the possibility of testing the Kerr-nature of astrophysical BH candidates by studying the properties of the electromagnetic radiation emitted by the gas of the accretion disk, for which there are already available data. In the last 5-8 years, there have been significant progresses in the understanding of the accretion process onto BH candidates and astronomers have developed several approaches to estimate the spin parameter of these objects under the assumption of Kerr background. One can typically extend these techniques to constrain/discover possible deviations from the Kerr metric (Bambi 2011d).

The content of the paper is as follows. In Section 2, I review the theoretical framework to test the Kerr-nature of astrophysical BH candidates: the Novikov-Thorne model, which can be used to describe thin accretion disks in generic stationary and axisymmetric space-times, and the choice of a non-Kerr background metric to parametrize possible deviations from the Kerr solution. In Section 3, I show some approaches to probe the geometry of

the space-time around astrophysical BH candidates from the analysis of the electromagnetic radiation emitted by the gas of accretion: the estimate of the radiative efficiency of AGNs, which can provide a rough idea of the size of deformations that may already be considered unlikely, the continuum-fitting method and the broad $K\alpha$ iron line analysis, which are the two most popular techniques currently used by astronomers to estimate the spin parameter of these objects and can be naturally extended to constrain possible deviations from the Kerr background, the high-frequency quasi-periodic oscillations (QPOs) and the estimate of the jet power, which may potentially be powerful probes, but in both cases the associated physical mechanism is not yet well understood from the theoretical point of view. Throughout the paper, I use units in which $G_N = c = 1$, unless stated otherwise.

2. Accretion process onto a compact object

2.1. Novikov-Thorne model

Geometrically thin and optically thick accretion disks are described by the Novikov-Thorne (NT) model (Novikov & Thorne 1973; Page & Thorne 1974), which is the relativistic generalization of the Shakura-Sunyaev model (Shakura & Sunyaev 1973). The disk is thin in the sense that the disk opening angle is $h = H/r \ll 1$, where H is the thickness of the disk at the radius r . In the Kerr background, there are four parameters (BH mass M , BH spin parameter a_* , mass accretion rate \dot{M} , and viscosity parameter α), but the model can be easily extended to any (quasi-)stationary, axisymmetric, and asymptotically flat space-time. Accretion is possible because viscous magnetic/turbulent stresses and radiation transport energy and angular momentum outwards. The model assumes that the disk is on the equatorial plane and that the disk's gas moves on nearly geodesic circular orbits. For long-term accretions, the disk is adjusted on the equatorial plane as a result of the Bardeen-Petterson effect (Bardeen & Petterson 1975) (such a mechanism works even in non-Kerr backgrounds (Bambi 2011a)). In the case of BH candidates in X-ray binaries, the disk is likely on the equatorial plane if the two bodies formed from the collapse of the same cloud (Fragos et al. 2010). The assumption of nearly geodesic circular orbits requires that the radial pressure is negligible compared to the gravitational force of the BH, which is indeed the case for thin disks. Heat advection is ignored (it scales as $\sim h^2$) and energy is radiated from the disk surface. Magnetic fields are also ignored.

The key-ingredient of the NT model is that the inner edge of the disk is at the innermost stable circular orbit (ISCO), where viscous stresses are assumed to vanish. When the gas's particles reach the ISCO, they quickly plunge into the BH, without emitting additional

radiation. At first approximation, the *total efficiency* of the accretion process is

$$\eta_{\text{tot}} = 1 - E_{\text{ISCO}}, \quad (1)$$

where E_{ISCO} is the specific energy of the gas at the ISCO radius and depends uniquely on the background geometry (see Appendix). In general, the total power of the accretion process is converted into radiation and kinetic energy of jet/wind outflows, so we can write $\eta_{\text{tot}} = \eta_{\text{rad}} + \eta_{\text{kin}}$, but in the NT model $\eta_{\text{kin}} = 0$. η_{rad} is the *radiative efficiency* and can be inferred from the bolometric luminosity L_{bol} if the mass accretion rate is known: $L_{\text{bol}} = \eta_{\text{rad}}\dot{M}$.

How good is the NT model to describe the accretion disk around astrophysical BH candidates? For non-magnetized and weakly-magnetized disks, there is a common consensus that the NT model describes correctly thin disks, $h \ll 1$, when the viscosity parameter is small, $\alpha \ll 1$ (Afshordi & Paczyński 2003). A common criterion to select sources with thin disks is that the bolometric to Eddington luminosity ratio, $L_{\text{bol}}/L_{\text{Edd}}$, does not exceed 0.3 (McClintock et al. 2006). In the case of magnetized disks, the issue is open and controversial. The GRMHD simulations in Penna et al. (2010) (see also Penna et al. (2012)) show that the stress at the inner edge of the disk scales as h and the authors conclude that the NT model with vanishing stress boundary condition is recovered for $h \rightarrow 0$. The GRMHD simulations in Noble & Krolik (2009) and Noble et al. (2010) show instead large stress at the inner edge of the disk even when $h \rightarrow 0$; according to these authors, the NT model cannot describe magnetized disks, even when the disk is very thin. It is not clear if the disagreement between the two groups can be attributed to different configurations of the magnetic fields, different resolution of the simulations, or something else.

2.2. Parametrizing deviations from the Kerr geometry

In the weak-field limit, General Relativity has been successfully tested in many situations. Solar System’s experiments are conveniently discussed within the parametrized post-Newtonian (PPN) formalism. One can see that the weak-field limit of a general static and spherically symmetric metric can be put in the form

$$ds^2 = - \left(1 - \frac{2M}{r} + 2\beta \frac{M^2}{r^2} + \dots \right) dt^2 + \left(1 + 2\gamma \frac{M}{r} + \dots \right) (dx^2 + dy^2 + dz^2), \quad (2)$$

where β and γ are the PPN parameters. In General Relativity, $\beta = \gamma = 1$, but in other metric theories of gravity that may not be true. Observations can measure β and γ and thus constrain possible deviations from the predictions of General Relativity.

The natural extension of the PPN formalism to test the space-time geometry around astrophysical BH candidates, where gravity is strong, is to write a general stationary, ax-

isymmetric, and asymptotically flat metric in terms of the mass moments, \mathcal{M}_l , and of the current moments, \mathcal{S}_l , of the compact object (Ryan 1995). In the case of a Kerr BH, all the moments are locked to the mass and angular momentum by the following relation (Hansen 1974):

$$\mathcal{M}_l + i\mathcal{S}_l = M \left(\frac{iJ}{M} \right)^l . \quad (3)$$

By measuring at least three non-trivial multiple moments of the space-time around an astrophysical BH candidate, one can test the Kerr-nature of the body. The advantage of a post-Newtonian approach is that we do not need specific assumptions about the nature of the BH candidate. The disadvantage is that we can only probe the metric relatively far from the compact object, where the contribution of higher-order moments can be neglected, and therefore we need very accurate measurements, which may not be possible in a realistic astrophysical situation.

In order to test the space-time geometry close to a BH candidate, we can consider a metric describing the gravitational field (in General Relativity or in an alternative theory of gravity) of a compact object characterized by its mass, its spin angular momentum, and a set of deformation parameters measuring possible deviations from the Kerr solution. In this way, one can compare observations and theoretical predictions in this more general background and check if the observations require that all the deformation parameters must vanish, as necessary if the space-time geometry around the BH candidate is really described by the Kerr metric. In the simplest case, we can consider just one deformation parameter, which should be able to describe the gravitational field around a compact object either more oblate or more prolate (according to the sign of the deformation parameter) than a Kerr BH. If our metric does it, it is not very important if it is an exact solution of the vacuum Einstein's equations (in this case, we are actually considering the possibility the BH candidate is a compact object made of exotic matter) or not, in the sense that we eventually get the same qualitative constraints (Bambi 2011e, 2012a; Li & Bambi 2012). In this review paper, I will focus the discussion on the metric proposed by Johannsen and Psaltis (JP) to describe the gravitational field around non-Kerr BHs in putative alternative theories of gravity (Johannsen & Psaltis 2011b). In Boyer-Lindquist coordinates, the JP metric is given by the line element

$$\begin{aligned} ds^2 = & - \left(1 - \frac{2Mr}{\Sigma} \right) (1 + h) dt^2 + \\ & + \frac{\Sigma(1 + h)}{\Delta + a^2 h \sin^2 \theta} dr^2 + \Sigma d\theta^2 - \frac{4aMr \sin^2 \theta}{\Sigma} (1 + h) dt d\phi + \\ & + \left[\sin^2 \theta \left(r^2 + a^2 + \frac{2a^2 Mr \sin^2 \theta}{\Sigma} \right) + \frac{a^2 (\Sigma + 2Mr) \sin^4 \theta}{\Sigma} h \right] d\phi^2 , \quad (4) \end{aligned}$$

where $a = a_*M$, $\Sigma = r^2 + a^2 \cos^2 \theta$, $\Delta = r^2 - 2Mr + a^2$, and

$$h = \sum_{k=0}^{\infty} \left(\epsilon_{2k} + \frac{Mr}{\Sigma} \epsilon_{2k+1} \right) \left(\frac{M^2}{\Sigma} \right)^k. \quad (5)$$

This metric has an infinite number of deformation parameters ϵ_i and the Kerr solution is recovered when all the deformation parameters are set to zero. However, in order to reproduce the correct Newtonian limit, we have to impose $\epsilon_0 = \epsilon_1 = 0$, while ϵ_2 is strongly constrained by Solar System experiments (Johannsen & Psaltis 2011b). In what follows, I will examine only the simplest case in which $\epsilon_3 \neq 0$, while all the other deformation parameters are set to zero.

3. Testing the Kerr-nature of BH candidates

3.1. Radiative efficiency of AGNs

The value of the spin parameter of a compact object is determined by the competition of three physical processes: the event creating the object, mergers, and gas accretion. Accretion from a disk can potentially be a very efficient way to spin a compact object up. If the inner edge of the disk is at the ISCO radius, the gas's particles plunge into the compact object with specific energy E_{ISCO} and specific angular momentum L_{ISCO} . The mass M and the spin angular momentum J of the compact object change respectively by $\delta M = E_{\text{ISCO}} \delta m$ and $\delta J = L_{\text{ISCO}} \delta m$, where δm is the gas rest-mass. The evolution of the spin parameter turns out to be governed by the following equation (Bardeen 1970)

$$\frac{da_*}{d \ln M} = \frac{1}{M} \frac{L_{\text{ISCO}}}{E_{\text{ISCO}}} - 2a_*, \quad (6)$$

neglecting the small effect of the radiation emitted by the disk and captured by the object. Prolonged disk accretion is a very efficient mechanism to spin the compact object up till an equilibrium spin parameter a_*^{eq} , which is reached when the right-hand side of Eq. (6) vanishes. For instance, an initially non-rotating Kerr BH reaches the equilibrium $a_*^{\text{eq}} = 1$ after having increased its mass by a factor $\sqrt{6} \approx 2.4$ (Bardeen 1970).

One can argue that the most favorable scenario to produce fast-rotating super-massive objects at the center of galaxies is likely via prolonged disk accretion and that the maximum value for the spin parameter of these objects today cannot exceed a_*^{eq} (Bambi 2011e). The numerical value of a_*^{eq} depends on the metric of the space-time and it may exceed 1, as the bound $|a_*| \leq 1$ holds for Kerr BHs (Bambi 2011a,c; Bambi & Modesto 2011). The black solid curve in Figure 1 shows the equilibrium spin parameter for the JP metric with deformation

parameter ϵ_3 . Objects on the left of the black solid curve have $a_* < a_*^{\text{eq}}$ and the accretion process spins them up; objects on the right have $a_* > a_*^{\text{eq}}$ and the accretion process spins them down.

In general, it is not easy to get an estimate of the radiative efficiency η_{rad} , as the measurement of the mass accretion rate \dot{M} is typically quite problematic. The mean radiative efficiency of AGNs can be inferred from the Soltan’s argument (Soltan 1982), which relates the mass density of the super-massive BH candidates in the contemporary Universe with the energy density of the radiation produced in the whole history of the Universe by the accretion process onto these objects. There are several sources of uncertainty in the final result, but a mean radiative efficiency $\eta_{\text{rad}} > 0.15$ seems to be a conservative lower limit (Elvis et al. 2002). Wang et al. (2006) find a mean radiative efficiency $\eta_{\text{rad}} \approx 0.30 - 0.35$ without some important assumptions necessary in the original version of the Soltan’s argument. Davis & Laor (2011) show how to estimate η_{rad} for individual AGNs and find that the most massive objects have typically higher η_{rad} , up to $\sim 0.3 - 0.4$.

It seems plausible to conclude that at least some of the super-massive BH candidates must have $\eta_{\text{rad}} > 0.15$. While the accretion disk of these objects may not be necessary thin, accretion from a thin disk is among the most efficient ways to convert the rest-mass of the gas into radiation. As $\eta_{\text{tot}} \geq \eta_{\text{rad}}$, $E_{\text{ISCO}} < 0.85$ and we can constrain deviations from the Kerr geometry (Bambi 2011b,e). A simplified explanation of how this is possible is the following. E_{ISCO} and a_*^{eq} increase/decrease if the gravitational force around the object increases/decreases, because the latter moves the ISCO to larger/smaller radii. Under the conservative assumption that $\eta_{\text{tot}} = \eta_{\text{rad}}$, we can compute η_{tot} of the background metric and, combining this bound with the one for the maximum value of the spin parameter as a function of the deformation parameter, we get a well defined allowed region in the spin parameter-deformation parameter plane. In the specific case of the JP metric with deformation parameter ϵ_3 , we find the plot in Figure 1. While the specific value of the deformation parameter depends on the choice of the metric of the background and a physical interpretation is not straightforward, the maximum value for the spin parameter seems to depend only very weakly on the exact space-time, which makes this argument quite appealing (Bambi 2011e). The maximum value today of the spin parameter for the super-massive BH candidates in galactic nuclei would be 1.19 if we require $\eta_{\text{tot}} > 0.15$, 1.10 for $\eta_{\text{tot}} > 0.20$, and 1.04 for $\eta_{\text{tot}} > 0.25$.

More recently, Li & Bambi (2012) have studied the accretion process from thick disks. While in this case the details strongly depend on the unknown properties of the accretion flow, at least in principle a thick disk can spin up a BH candidate more efficiently. The evolution of the spin parameter is still given by Eq. (6), but the quantity $L_{\text{ISCO}}/E_{\text{ISCO}}$ is replaced

by $L_{\text{in}}/E_{\text{in}}$, where E_{in} and L_{in} are, respectively, the specific energy and the specific angular momentum of the gas particles at the inner edge of the disk. For a thick disk, the inner edge of the disk can be inside the ISCO. So, if the super-massive BH candidates have experienced a period of super-Eddington accretion in the recent past, their spin parameter might exceed the equilibrium value a_*^{eq} computed from a thin disk. Under the most conservative assumptions, the previous bounds on the maximum value of a_* become slightly weaker: 1.30 for $\eta_{\text{tot}} > 0.15$, 1.18 for $\eta_{\text{tot}} > 0.20$, and 1.10 for $\eta_{\text{tot}} > 0.25$ (Li & Bambi 2012).

3.2. Continuum-fitting method

In the NT model, the thermal spectrum of a geometrically thin and optically thick accretion disk around a Kerr BH observed far from the compact object depends on 5 parameters: BH mass M , BH distance d , inclination angle of the disk with respect to the line of sight of the observer i , BH mass accretion rate \dot{M} , and BH spin a_* . If we can get independent measurements of M , d , and i , we can fit the data and estimate \dot{M} and a_* . The technique is called continuum-fitting method (Zhang et al. 1997; Li et al. 2005; McClintock et al. 2011) and it can be applied only to stellar-mass BH candidates: the disk’s temperature goes like $M^{-0.25}$, and the peak of the spectrum is at about 1 keV for $M \sim 10 M_{\odot}$ and in the UV range for super-massive objects in galactic nuclei. In the latter case, a good measurement is impossible because of dust absorption. From the conservation laws for the rest-mass, angular momentum and energy, one can deduce three basic equations for the time-averaged radial structure of the disk. In particular, the time-averaged energy flux emitted from the surface of the disk is (Page & Thorne 1974)

$$\mathcal{F}(r) = \frac{\dot{M}}{4\pi M^2} F(r), \quad (7)$$

where $F(r)$ is the dimensionless function

$$F(r) = -\frac{\partial_r \Omega}{(E - \Omega L)^2} \frac{M^2}{\sqrt{-G}} \int_{r_{\text{in}}}^r (E - \Omega L)(\partial_\rho L) d\rho. \quad (8)$$

E , L , and Ω are, respectively, the conserved specific energy, the conserved axial-component of the specific angular momentum, and the angular velocity for equatorial circular geodesics (see Appendix); $G = -\alpha^2 g_{rr} g_{\phi\phi}$ is the determinant of the near equatorial plane metric, where $\alpha^2 = g_{t\phi}^2/g_{\phi\phi} - g_{tt}$ is the lapse function; r_{in} is the inner radius of the accretion disk and in the NT model it is the ISCO radius.

Since the disk is in thermal equilibrium, the emission is blackbody-like and we can define an effective temperature $T_{\text{eff}}(r)$ from the relation $\mathcal{F}(r) = \sigma T_{\text{eff}}^4$, where σ is the Stefan-Boltzmann constant. Actually, the disk's temperature near the inner edge of the disk can be high, up to $\sim 10^7$ K for stellar-mass BH candidates, and non-thermal effects are non-negligible. That is usually taken into account by introducing the color factor (or hardening factor) f_{col} . The color temperature is $T_{\text{col}}(r) = f_{\text{col}} T_{\text{eff}}$ and the local specific intensity of the radiation emitted by the disk is

$$I_e(E_e) = \frac{2E_e^3}{h^2 c^2} \frac{1}{f_{\text{col}}^4} \frac{\Upsilon}{\exp\left(\frac{E_e}{k_B T_{\text{col}}}\right) - 1}, \quad (9)$$

where E_e is the photon energy, h is the Planck's constant, c is the speed of light, k_B is the Boltzmann constant, and Υ is a function of the angle between the 3-momentum of the photon emitted by the disk and the normal of the disk surface, say ξ . The two most common options are $\Upsilon = 1$ (isotropic emission) and $\Upsilon = \frac{1}{2} + \frac{3}{4} \cos \xi$ (limb-darkened emission).

The calculation of the thermal spectrum of a thin accretion disk has been extensively discussed in the literature; see e.g. Li et al. (2005) and references therein for the Kerr case, and Bambi & Barausse (2011a), Chen & Jing (2012a) and Bambi (2012f) for a background with generic deviations from the Kerr solution. The spectrum can be conveniently written in terms of the photon flux number density as measured by a distant observer, $N_{E_{\text{obs}}}$. In the case of non-Kerr background, it is convenient to use a ray-tracing approach. The initial conditions $(t_0, r_0, \theta_0, \phi_0)$ for the photon with Cartesian coordinates (X, Y) on the image plane of the distant observer are given by (Johannsen & Psaltis 2010)

$$t_0 = 0, \quad (10)$$

$$r_0 = \sqrt{X^2 + Y^2 + d^2}, \quad (11)$$

$$\theta_0 = \arccos \frac{Y \sin i + d \cos i}{\sqrt{X^2 + Y^2 + d^2}}, \quad (12)$$

$$\phi_0 = \arctan \frac{X}{d \sin i - Y \cos i}. \quad (13)$$

As the initial 3-momentum \mathbf{k}_0 must be perpendicular to the plane of the image of the

observer, the initial conditions for the 4-momentum of the photon are

$$k_0^r = -\frac{d}{\sqrt{X^2 + Y^2 + d^2}} |\mathbf{k}_0|, \quad (14)$$

$$k_0^\theta = \frac{\cos i - d \frac{Y \sin i + d \cos i}{X^2 + Y^2 + d^2}}{\sqrt{X^2 + (d \sin i - Y \cos i)^2}} |\mathbf{k}_0|, \quad (15)$$

$$k_0^\phi = \frac{X \sin i}{X^2 + (d \sin i - Y \cos i)^2} |\mathbf{k}_0|, \quad (16)$$

$$k_0^t = \sqrt{(k_0^r)^2 + r_0^2 (k_0^\theta)^2 + r_0^2 \sin^2 \theta_0 (k_0^\phi)^2}, \quad (17)$$

where k_0^t is inferred from the condition $g_{\mu\nu} k^\mu k^\nu = 0$ with the metric tensor of a flat space-time (as the observer is located far from the compact object). The photon trajectory is numerically integrated backwards in time to the point of the photon emission on the accretion disk: in this way, we get the radial coordinate r_e at which the photon was emitted and the angle ξ between the 3-momentum of the photon and the normal of the disk surface (necessary to compute Υ).

The observer's sky is divided into a number of small elements and the ray-tracing procedure provides the observed flux density from each element; summing up all the elements, we get the total observed flux density of the disk. In the case of Kerr background, one can actually exploit the special properties of the Kerr solution and solve a simplified set of differential equations. That is not possible in a generic non-Kerr background and one has to solve the second-order photon geodesic equations of the space-time. The photon flux number density is given by

$$\begin{aligned} N_{E_{\text{obs}}} &= \frac{1}{E_{\text{obs}}} \int I_{\text{obs}}(E_{\text{obs}}) d\Omega_{\text{obs}} = \frac{1}{E_{\text{obs}}} \int g^3 I_e(E_e) d\Omega_{\text{obs}} = \\ &= A_1 \left(\frac{E_{\text{obs}}}{\text{keV}} \right)^2 \int \frac{1}{M^2} \frac{\Upsilon dX dY}{\exp \left[\frac{A_2}{g F^{1/4}} \left(\frac{E_{\text{obs}}}{\text{keV}} \right) \right] - 1}, \end{aligned} \quad (18)$$

where I_{obs} and E_{obs} are, respectively, the specific intensity of the radiation and the photon energy measured by the distant observer. $d\Omega_{\text{obs}} = dX dY / d^2$ is the element of the solid angle subtended by the image of the disk on the observer's sky. g is the redshift factor

$$g = \frac{E_{\text{obs}}}{E_e} = \frac{k_\alpha u_{\text{obs}}^\alpha}{k_\beta u_e^\beta}, \quad (19)$$

where k^α is the 4-momentum of the photon, $u_{\text{obs}}^\alpha = (-1, 0, 0, 0)$ is the 4-velocity of the distant observer, and $u_e^\alpha = (u_e^t, 0, 0, \Omega u_e^t)$ is the 4-velocity of the emitter. $I_e(E_e)/E_e^3 = I_{\text{obs}}(E_{\text{obs}})/E_{\text{obs}}^3$

follows from the Liouville's theorem. A_1 and A_2 are given by (for the sake of clarity, here I show explicitly G_N and c)

$$\begin{aligned}
 A_1 &= \frac{2(\text{keV})^2}{f_{\text{col}}^4} \left(\frac{G_N M}{c^3 h d} \right)^2 = \\
 &= \frac{0.07205}{f_{\text{col}}^4} \left(\frac{M}{M_\odot} \right)^2 \left(\frac{\text{kpc}}{d} \right)^2 \gamma \text{keV}^{-1} \text{cm}^{-2} \text{s}^{-1}, \\
 A_2 &= \left(\frac{\text{keV}}{k_B f_{\text{col}}} \right) \left(\frac{G_N M}{c^3} \right)^{1/2} \left(\frac{4\pi\sigma}{\dot{M}} \right)^{1/4} = \\
 &= \frac{0.1331}{f_{\text{col}}} \left(\frac{10^{18} \text{g s}^{-1}}{\dot{M}} \right)^{1/4} \left(\frac{M}{M_\odot} \right)^{1/2}.
 \end{aligned} \tag{20}$$

Using the normalization condition $g_{\mu\nu} u_e^\mu u_e^\nu = -1$, one finds

$$u_e^t = -\frac{1}{\sqrt{-g_{tt} - 2g_{t\phi}\Omega - g_{\phi\phi}\Omega^2}}, \tag{21}$$

and therefore

$$g = \frac{\sqrt{-g_{tt} - 2g_{t\phi}\Omega - g_{\phi\phi}\Omega^2}}{1 + \lambda\Omega}, \tag{22}$$

where $\lambda = k_\phi/k_t$ is a constant of the motion along the photon path and can be evaluated from the photon initial conditions ($\lambda = k_\phi/k_t = r_0 \sin\theta_0 k_0^\phi/k_0^t$).

Figure 2 shows the thermal spectrum of a thin disk as a function of the parameters of the model. M , d , and i should be inferred from independent measurements, while a_* , \dot{M} , and ϵ_3 can be obtained by fitting the disk's spectrum. It is evident that variations of a_* and ϵ_3 produce quite similar effects on the shape of the spectrum, while \dot{M} changes the spectrum in a very different way. Figure 3 shows the effects of variations of the color factor f_{col} (typically one should expect $f_{\text{col}} = 1.6 - 1.7$) and of the function Υ (whose effect is relevant only for large inclination angles).

In order to figure out how the analysis of the thermal spectrum of a thin disk can constrain the geometry of the space-time around a BH candidate, we can compare the spectra of a Kerr BH and of a JP BH with deformation parameter ϵ_3 . We define the reduced χ^2 as follows

$$\chi_{\text{red}}^2(a_*, \epsilon_3, \dot{M}) = \frac{\chi^2}{n} = \frac{1}{n} \sum_{i=1}^n \frac{\left[N_i^{\text{JP}}(a_*, \epsilon_3, \dot{M}) - N_i^{\text{Kerr}}(\tilde{a}_*, \tilde{M}) \right]^2}{\sigma_i^2}, \tag{23}$$

where the summation is performed over n sampling energies E_i , N_i^{JP} and N_i^{Kerr} are the photon flux number densities respectively for the JP and Kerr metric, and σ_i is the uncertainty. As

variations of \dot{M} produce quite different effects on the shape of the spectrum with respect to a_* and ϵ_3 , its determination is not correlated to the other two parameters and here we directly assume $\dot{M} = \tilde{M}$. Figure 4 shows χ_{red}^2 for two cases: $\tilde{a}_* = 0.7$ (left panel) and $\tilde{a}_* = 0.98$ (right panel), assuming that the uncertainty is 10% the photon flux number density; that is, $\sigma_i = 0.1 N_i^{\text{Kerr}}$. The continuum-fitting method basically measures the radiative efficiency $\eta_{\text{rad}} = 1 - E_{\text{ISCO}}$, not the spin parameter a_* . In the Kerr metric, η_{rad} depends only on a_* and therefore one can infer the spin of the compact object. In a generic non-Kerr background, one can only measure a combination of a_* and of the deformation parameters. The technique is indeed unable to distinguish a Kerr BH with spin parameter \tilde{a}_* from a very deformed object with completely different spin parameter but very similar radiative efficiency (Bambi & Barausse 2011a). An analysis of real data from specific sources will be presented in Bambi et al. (2013).

For the time being, the continuum-fitting method has been used to estimate the spin parameter of 9 stellar-mass BH candidates under the assumption that these objects are Kerr BHs. The list of these objects is reported in Table 1. There are 2 objects that look like very fast-rotating Kerr BHs (GRS 1915+105 and Cygnus X-1), 4 objects that seem to be Kerr BHs with a mid value of the spin parameter (LMC X-1, M33 X-7, 4U 1543-47, and GRO J1655-40), and 3 objects whose data are consistent with slow-rotating Kerr BHs (XTE J1550-564, LMC X-3, and A0620-00). The measure of the spin parameter a_* under the Kerr BH hypothesis can be quickly translated into a measurement of η_{rad} and then into an allowed region on the spin parameter-deformation parameter plane, see Fig. 5. The comparison of the allowed region for GRO J1655-40 (black area, right panel in Figure 5) with the χ_{red}^2 in the left panel of Figure 4 shows that the continuum-fitting method measures indeed the radiative efficiency. For high values of the spin and of the deformation parameters, the rule of the radiative efficiency does not work so well (see the case of GRS 1915+105 or Cygnus X-1 and compare with the allowed region in the right panel of Figure 4), but such a region of the plane is more likely unphysical, as it is probably impossible to spin these very prolate compact objects to so high values of a_* (see e.g. the black line in Figure 1).

3.3. Broad $K\alpha$ iron line

The X-ray spectrum of both stellar-mass and super-massive BH candidates is often characterized by the presence of a power-law component. This feature is commonly interpreted as the inverse Compton scattering of thermal photons by electrons in a hot corona above the accretion disk. The geometry of the corona is not known and several models have been proposed. Such a “primary component” irradiates the accretion disk, producing a “reflec-

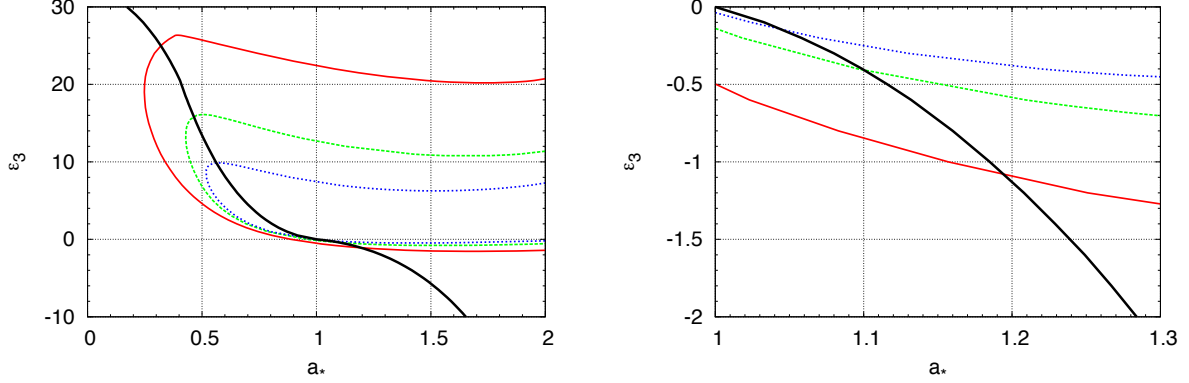


Fig. 1.— Total efficiency $\eta_{\text{tot}} = 1 - E_{\text{ISCO}}$ in the JP background with spin parameter a_* and deformation parameter ϵ_3 . $\eta_{\text{tot}} = 0.15$ (red solid curve), 0.20 (green dashed curve), and 0.25 (blue dotted curve). The black solid curve is the equilibrium spin parameter a_*^{eq} obtained from Eq. (6). The right panel is an enlargement of the parameter region $1.0 < a_* < 1.3$ and $-2.0 < \epsilon_3 < 0.0$.

BH Binary	a_*^{Kerr}	η_{min}	η_{max}	Reference
GRS 1915+105	$a_* > 0.98$	0.234	0.423	McClintock et al. (2006)
Cygnus X-1	$a_* > 0.97$	0.215	0.423	Gou et al. (2011)
LMC X-1	0.92 ± 0.06	0.139	0.234	Gou et al. (2009)
M33 X-7	0.84 ± 0.05	0.120	0.151	Liu et al. (2008, 2010)
4U 1543-47	0.80 ± 0.05	0.112	0.136	Shafee et al. (2006)
GRO J1655-40	0.70 ± 0.05	0.097	0.112	Shafee et al. (2006)
XTE J1550-564	0.34 ± 0.24	0.0606	0.0892	Steiner et al. (2011)
LMC X-3	$a_* < 0.3$	0.0365	0.0694	Davis et al. (2006)
A0620-00	0.12 ± 0.19	0.0550	0.0699	Gou et al. (2010)

Table 1: Continuum-fitting method results from the Harvard-Smithsonian CfA group. See references in the last column for more details.

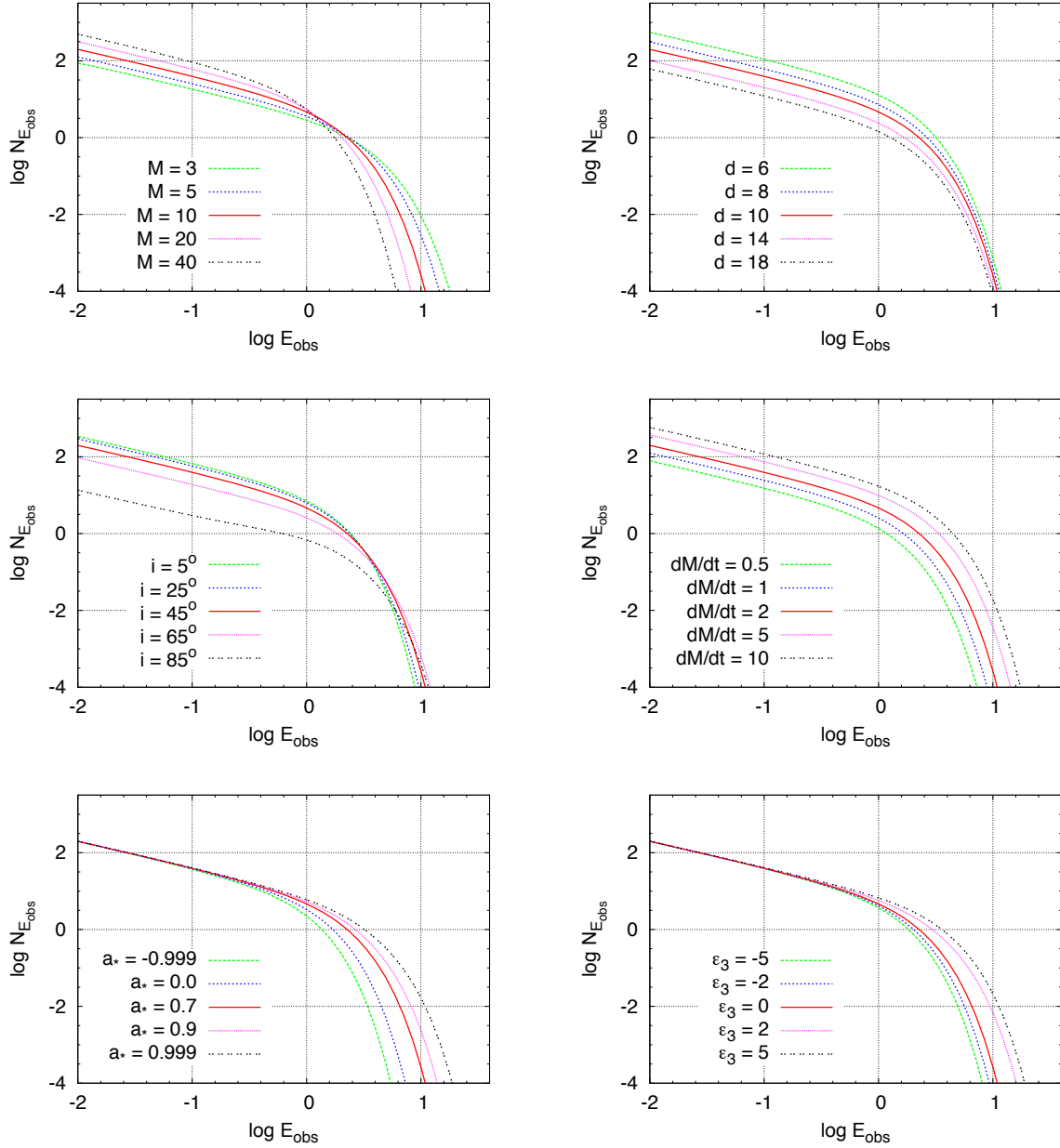


Fig. 2.— Thermal spectrum of a thin disk as a function of the parameters of the model. Left top panel: mass of the BH candidate in units of M_{\odot} . Right top panel: distance of the BH candidate in kpc. Left central panel: inclination angle of the disk with respect to the line of sight of the distant observer. Right central panel: mass accretion rate in units of 10^{18} g s^{-1} . Left bottom panel: spin parameter of the BH candidate. Right bottom panel: deformation parameter of the BH candidate. When not shown, the value of the parameters is: $M = 10 M_{\odot}$, $d = 10 \text{ kpc}$, $i = 45^{\circ}$, $\dot{M} = 2 \cdot 10^{18} \text{ g s}^{-1}$, $a_* = 0.7$, $\epsilon_3 = 0.0$. Flux density $N_{E_{\text{obs}}}$ in $\gamma \text{ keV}^{-1} \text{ cm}^{-2} \text{ s}^{-1}$; photon energy E_{obs} in keV.

tion component” in the X-ray spectrum. The illumination of the cold disk by the primary component produces also spectral lines by fluorescence. The strongest line is the $K\alpha$ iron line at 6.4 keV. This line is intrinsically narrow in frequency, while the one observed appears broadened and skewed. The interpretation is that the line is strongly altered by special and general relativistic effects, which produce a characteristic profile, first predicted in Fabian et al. (1989) and then observed for the first time in the ASCA data of the Seyfert 1 galaxy MCG-6-30-15 (Tanaka et al. 1995). In MCG-6-30-15, this line is extraordinarily stable, in spite of a substantial variability of the continuum, suggesting that the analysis of its shape can be used to probe the geometry of the space-time around the BH candidate. However, the relativistic origin of the observed broad $K\alpha$ iron lines is not universally accepted, and some authors have proposed different explanations (Turner et al. 2007; Titarchuk et al. 2009).

Within the interpretation of a relativistically broadened $K\alpha$ iron line, the shape of the line is primarily determined by the background metric, the geometry of the emitting region, the disk emissivity, and the disk’s inclination angle with respect to the line of sight of the distant observer (Fabian et al. 1989; Reynolds & Nowak 2003; Miller 2007). The effects of deviations from the Kerr metric on the shape of the $K\alpha$ iron line are discussed in Psaltis & Johannsen (2012), Johannsen & Psaltis (2012), and Bambi (2013). In Kerr and non-Kerr backgrounds, M sets the length of the system, so everything scales as M or as some power of M , without affecting the shape of the line. The relevant parameters of the background geometry are thus the spin a_* and possible non-vanishing deformation parameters. In those sources for which there is indication that the $K\alpha$ iron line is mainly emitted close to the compact object, the emission region may be thought to range from the ISCO radius, $r_{\text{in}} = r_{\text{ISCO}}$, to some outer radius r_{out} . However, even more complicated geometries have been proposed (Martocchia et al. 2000). In principle, the disk emissivity may be theoretically calculated. In practice, that is not feasible at present. The simplest choice is an intensity profile $I_e \propto r^\alpha$, with $\alpha < 0$ a free parameter to be determined during the fitting procedure.

The line spectra can be expressed in terms of the photon flux number density as measured by the distant observer:

$$N_{E_{\text{obs}}} = \frac{1}{E_{\text{obs}}} \int I_{\text{obs}}(E_{\text{obs}}) d\Omega_{\text{obs}} = \frac{1}{E_{\text{obs}}} \int g^3 I_e(E_e) d\Omega_{\text{obs}}. \quad (24)$$

Let us assume that the disk emission is monochromatic (the rest frame energy is $E_{K\alpha} = 6.4$ keV) and isotropic with a power-law radial profile:

$$I_e(E_e) \propto \delta(E_e - E_{K\alpha}) r^\alpha. \quad (25)$$

The resulting broad $K\alpha$ iron lines for different values of the model parameters (spin a_* , deformation ϵ_3 , inclination angle i , power-law index α , and outer radius r_{out}) are shown in

Figure 6. The photon flux has been normalized so that

$$\int N_{E_{\text{obs}}} dE_{\text{obs}} = \text{constant}, \quad (26)$$

as only the shape matters.

As we can see in Figure 6, the effect of variations of a_* and of the deformation parameter ϵ_3 is similar. For small deformations, backgrounds with the same efficiency in the NT model, $\eta_{\text{rad}} = 1 - E_{\text{ISCO}}$, have similar broad $K\alpha$ iron lines and it is difficult to distinguish a Kerr BH from another compact object (see the right bottom panel). However, unlike in the case of the thermal spectrum of a thin disk, for larger deformations that is not true any more. The location of the ISCO radius (set by a_* and ϵ_3 and determining η_{rad}) is encoded in the low-energy tail of the broad line. It consists of photons emitted from the receding part of the accretion disk close to the inner edge and thus strongly affected by both gravitational and Doppler redshift. The main peak of the line is produced by the effect of Doppler blueshift, relatively far from the compact object, where the effect of gravitational redshift is not so strong. For small values of the deformation parameters, the Keplerian velocity profile is still similar to the one of a Kerr BH and an object with similar radiative efficiency may look like a Kerr BH with different spin parameter. For larger deviations from the Kerr background, the role of the Doppler boosting (in both the main peak and the low-energy tail) becomes more and more important and breaks the degeneracy between spin and deformation parameter. To be more quantitative, we can proceed as in the previous section and compare the line produced in the space-time around a Kerr BH and a deformed object. The reduced χ^2 is now:

$$\chi_{\text{red}}^2(a_*, \epsilon_3, i, \alpha, r_{\text{out}}) = \frac{\chi^2}{n} = \frac{1}{n} \sum_{i=1}^n \frac{[N_i^{\text{JP}}(a_*, \epsilon_3, i, \alpha, r_{\text{out}}) - N_i^{\text{Kerr}}(\tilde{a}_*, \tilde{i}, \tilde{\alpha}, \tilde{r}_{\text{out}})]^2}{\sigma_i^2}, \quad (27)$$

where the summation is performed over n sampling energies E_i , N_i^{JP} and N_i^{Kerr} are the normalized photon fluxes in the energy bin $[E_i, E_i + \Delta E]$, respectively for the JP and Kerr metric, and σ_i is the uncertainty of the energy bin. Motivated by the fact that variations of i , α , and r_{out} produce different effects on the shape of the line with respect to a_* and ϵ_3 , for the sake of simplicity we can fix $i = \tilde{i}$, $\alpha = \tilde{\alpha}$, and $r_{\text{out}} = \tilde{r}_{\text{out}}$ (actually, such an approximation may not be so good for the inclination angle, see Bambi (2013)). Assuming a 10% uncertainty in the photon count, i.e. $\sigma_i = 0.1 N_i^{\text{Kerr}}$, and data in the energy range 1 – 7.5 keV with an energy resolution $\Delta E = 100$ eV, we get the plots in Figure 7 for $\tilde{a} = 0.7$ (left panel) and 0.98 (right panel). Unlike for the analysis of the disk’s spectrum, here we can exclude that a source with a $K\alpha$ iron line that looks like the one generated in a Kerr space-time with spin parameter $\tilde{a} = 0.7$ comes instead from the region around a very deformed compact object.

It is also interesting to see what happens if we combine the analysis of the thermal spectrum of the disk with the one of the broad $K\alpha$ iron line. In general, it is not common to have good measurements of both the disk’s spectrum and the $K\alpha$ iron line for the same object, but it is possible and it may be more likely with future experiments. If we define

$$\chi_{\text{red, tot}}^2 = \chi_{\text{red, } K\alpha}^2 + \chi_{\text{red, cfm}}^2, \quad (28)$$

where $\chi_{\text{red, } K\alpha}^2$ and $\chi_{\text{red, cfm}}^2$ are, respectively, the reduced χ^2 defined in Eq. (27) and (23), we find the two plots shown in Figure 8.

3.4. Quasi Periodic Oscillations

The X-ray power density spectra of some low-mass X-ray binaries show some peaks; that is, there are QPOs in the X-ray flux (Remillard & McClintock 2006). These features can be observed in systems with both BH candidates and neutron stars and the frequencies of these oscillations are in the range 0.1 Hz–1 kHz. High-frequency QPOs in BH candidates (~ 40 -450 Hz) are particularly interesting, as they depend only very weakly on the observed X-ray flux and for this reason it is thought they are determined by the metric of the space-time rather than by the properties of the accretion flow. If that is correct, they may be used to probe the geometry around stellar-mass BH candidates. For the time being, however, the exact physical mechanism responsible for the production of the high-frequency QPOs is not known and several different scenarios have been proposed, including hot-spot models (Stella & Vietri 1998, 1999), diskoseismology models (Perez et al. 1997; Silbergleit et al. 2001; Wagoner et al. 2001; Kato 2001), resonance models (Abramowicz & Kluzniak 2001; Abramowicz et al. 2003; Kluzniak & Abramowicz 2005; Török et al. 2005), and p-mode oscillations of a small accretion torus (Rezzolla et al. 2003a,b; Schnittman & Rezzolla 2006). In these models, the frequencies of the QPOs are directly related to the three characteristic

BH binary	M/M_{\odot}	ν_U/Hz	ν_L/Hz	References
GRO J1655-40	6.30 ± 0.27	450 ± 3	300 ± 5	Strohmayer (2001)
XTE J1550-564	9.1 ± 0.6	276 ± 3	184 ± 5	Remillard et al. (2002)
GRS 1915+105	14.0 ± 4.4	168 ± 3	113 ± 5	Remillard & McClintock (2006)

Table 2: Stellar-mass BH candidates in binary systems with a measurement of the mass and two observed high-frequency QPOs.

orbital frequencies of a test-particle: the Keplerian frequency ν_K (which is the inverse of the orbital period), the radial epicyclic frequency ν_r (the frequency of radial oscillations around the mean orbit), and the vertical epicyclic frequency ν_θ (the frequency of vertical oscillations around the mean orbit). These three frequencies depend on the geometry of the space-time and on the radius of the orbit. While they are defined as the characteristic frequencies of the orbital motion for a free particle, there is a direct relation between these frequencies and the ones of the oscillation modes of the fluid accretion flow.

In the Kerr space-time, the radial epicyclic frequency ν_r reaches a maximum at some radius $r_{\max} > r_{\text{ISCO}}$ and then vanishes at the ISCO, as the orbit becomes marginally radially unstable. Keplerian and vertical epicyclic frequencies are instead defined up to the photon orbit. Circular orbits with radius smaller than the one of the photon orbit do not exist. $\nu_\theta > \nu_r$, and for corotating orbits $\nu_K \geq \nu_\theta$. If the space-time geometry around BH candidates is described by the Kerr metric, the measurement of the high-frequency QPOs may provide an estimate of the BH spin parameter, assuming the exact mechanism responsible for these oscillations is known. Török et al. (2011) compare the available spin measurements from high-frequency QPOs and the continuum-fitting method and find that the two approach do not provide consistent results if we believe that all the observed high-frequency QPOs can be explained within a unique model.

The high-frequency QPO models developed for the Kerr metric can be generalized to non-Kerr backgrounds (Johannsen & Psaltis 2011a; Aliev et al. 2012; Bambi 2012c). The possibility of the existence of vertically unstable orbits, absent in the Kerr space-time, allows for a larger number of possible combinations between different modes. $\nu_\theta > \nu_r$ is not true any more. The conflict between measurements from high-frequency QPOs and the continuum-fitting method can be solved within a unique astrophysical model by admitting that the geometry around BH candidates deviates from the Kerr solution (Bambi 2012c).

In four stellar-mass BH candidates, we observe two high-frequency QPOs. It is remarkable that in all the four cases the ratio of the two frequencies is 3:2, suggesting a strong correlation between them. Possible theoretical models should thus be able to explain this feature. The resonance models (Abramowicz & Kluzniak 2001; Abramowicz et al. 2003; Kluzniak & Abramowicz 2005; Török et al. 2005) seem to be quite appealing from this point of view. For a free particle, the radial and the vertical modes are decoupled (see Eqs. (A8) and (A9) in Appendix). However, it is natural to expect that in a more realistic description there are non-linear effects coupling the two epicyclic modes. In this case, the equations can

be written as

$$\frac{d^2\delta_r}{dt^2} + \Omega_r^2\delta_r = \Omega_r^2 F_r \left(\delta_r, \delta_\theta, \frac{d\delta_r}{dt}, \frac{d\delta_\theta}{dt} \right), \quad (29)$$

$$\frac{d^2\delta_\theta}{dt^2} + \Omega_\theta^2\delta_\theta = \Omega_\theta^2 F_\theta \left(\delta_r, \delta_\theta, \frac{d\delta_r}{dt}, \frac{d\delta_\theta}{dt} \right), \quad (30)$$

where F_r and F_θ are some functions that depend on the specific properties of the accretion flow. If we knew the details of the physical mechanisms of the accretion process, we could write the explicit form of these two functions and solve the system. Unfortunately, that is not the case. However, regardless of the specific resonance model and the microphysics responsible for it, the resonance paradigm requires that the upper and the lower frequencies have the form

$$\nu_U = m_1\nu_r + m_2\nu_\theta, \quad (31)$$

$$\nu_L = n_1\nu_r + n_2\nu_\theta. \quad (32)$$

where $m_1, m_2, n_1,$ and n_2 are integer (and likely as small as possible) numbers. Scenarios with a coupling between ν_r and ν_θ are surely theoretically more motivated, but it is not possible to exclude *a priori* that ν_U and ν_L actually arise from the combination of ν_K with one of the other two frequencies and have the form like $\nu_U = m_1\nu_K + m_2\nu_r$ and $\nu_L = n_1\nu_K + n_2\nu_r$. Assuming the JP background with deformation parameter ϵ_3 , we can compare the theoretical predictions with the observed ν_U and ν_L for any BH candidate and define an allowed region on the plane spin parameter-deformation parameter for any specific set of $\{m_1, m_2, n_1, n_2\}$.

While systematic effects and/or wrong models are surely the most likely possibility to explain the disagreement between the spin measurements obtained by the continuum-fitting method and the high-frequency QPOs, Bambi (2012c) explores the possibility of explaining all the observations with a unique astrophysical model in a non-Kerr background. It turns out that the resonance $\nu_\theta : \nu_r = 3 : 1$ can do the job if the JP deformation parameter ϵ_3 is in the range 5 to 15. In this scenario, GRO J1655-40 and XTE J1550-564 would be “slow-rotating” compact objects and their ISCO would be marginally radially stable. GRS 1915+105 would instead be a “fast-rotating” object with $a_* \approx 0.5$ and its ISCO would be marginally vertically stable.

3.5. Jet power

Jets and outflows are a quite common feature of accreting compact objects. In the case of stellar-mass BH candidates in X-ray binary systems, we observe two kinds of jets (Fender

et al. 2004). *Steady jets* occur in the hard spectral state. *Transient jets* appear most significantly when the source switches from the hard to the soft state. Most efforts so far concentrate on the formation mechanism of steady jets. One of the most appealing scenarios to explain the formation of steady jets is the Blandford-Znajek mechanism (Blandford & Znajek 1977), in which magnetic fields threading the BH event horizon are twisted and can extract the rotational energy of the spinning BH, producing an electromagnetic jet. Numerical simulations show that the mechanism can be very efficient and depends strongly on the BH spin (McKinney 2005; Tchekhovskoy et al. 2010, 2011). At the moment it is not clear if the Blandford-Znajek mechanism can be responsible for the production of steady jets, and in the literature there are some controversial results. The spin scenario is surely attractive, but still unproved.

Recently, there have been some studies investigating if there is observational evidence for a correlation between BH spin and jet power in current data. Fender et al. (2010) consider all the spin measurements of BH binaries reported in the literature from the continuum-fitting method and the $K\alpha$ iron line analysis. For steady jets in the hard spectral state, they estimate the jet power via a normalization C , defined by

$$\log_{10} L_{\text{radio}} = C + 0.6 (\log_{10} L_X - 34) , \quad (33)$$

where L_{radio} and L_X are, respectively, the radio and X-ray luminosity of the object. Their plots show no evidence for a correlation between BH spin and jet power. The left panel of Figure 9 shows the case in which the spin parameter is measured with the continuum-fitting method. If the measurements of the spins and of the jet powers are correct, it seems that steady jets are not powered by the BH spin.

Narayan & McClintock (2012) propose that the Blandford-Znajek mechanism is responsible for the formation of transient jets. They consider the most recent spin measurements of the continuum-fitting method from the Harvard-Smithsonian CfA group, which are supposed to be more reliable, and use a different proxy for the jet power, the peak radio flux normalized at 5 GHz, which they claim to be model independent. These authors find a correlation between BH spin a_* and jet power P_{jet} (see the right panel in Figure 9), which is consistent with both the theoretical prediction

$$P_{\text{jet}} \propto a_*^2 \quad (34)$$

obtained in Blandford & Znajek (1977) for $a_*^2 \ll 1$ and the more accurate one

$$P_{\text{jet}} \propto \Omega_{\text{H}}^2 \propto a_*^2 / r_{\text{H}}^2 , \quad (35)$$

where Ω_{H} and r_{H} are, respectively, the angular frequency and the radius of the event horizon, found in Tchekhovskoy et al. (2010) and valid even when a_* is quite close to 1. However, numerical studies of the Blandford-Znajek mechanism show the production of steady jets, while

the origin of transient jets remains unclear and other scenarios may look more promising, such as episodic ejections of plasma blobs (Yuan et al. 2009).

In Fender et al. (2010) and Narayan & McClintock (2012), the authors rely on spin measurements obtained under the assumption that BH candidates are Kerr BHs. If this hypothesis were wrong, all the spin measurements would be wrong too. On the contrary, a jet powered by the Blandford-Znajek mechanism should still be correlated with the spin of the compact object. The existence of the event horizon is not strictly necessary for the production of jets powered by the spin: for example, even neutron stars may have spin powered jets if there are magnetic fields anchored on the neutron star. On very general arguments, if the jet is powered by the rotational energy of the compact object, the power can be written as

$$P_{\text{jet}} = A_0 + \sum_{n=1}^{+\infty} A_n |a_*|^{2n}, \quad (36)$$

where A_0 takes into account a possible non-spin contribution ($A_0 \geq 0$, as P_{jet} cannot become negative for $a_* = 0$) and the other terms are due to (some version of) the Blandford-Znajek mechanism. The latter must depend only on even powers of a_* , because the direction of the spin should not be important (at least at first approximation).

Let us now examine the spin measurements obtained with the continuum-fitting method, as they can be easily translated into efficiency measurements in the NT model, and then into allowed regions on the spin parameter-deformation parameter plane. From Section 3.2, one can see that an object more prolate than a Kerr BH ($\epsilon_3 > 0$) may be interpreted as a Kerr BH with a higher value of the spin parameter. An object more oblate than a Kerr BH ($\epsilon_3 < 0$) has instead a spectrum similar to a Kerr BH with a lower value of a_* . While the jet power is independent of the spin sign, the continuum-fitting method is not, and the measurement of a very low radiative efficiency can be attributed to an object with a retrograde accretion disk.

If we believe that steady jets are powered by the spin of the compact object, we can see if a correlation between jet power and spin parameter is possible for a non-vanishing deformation parameter (Bambi 2012d). In the left panel of Figure 9, the absence of a correlation between a_* and P_{jet} is essentially due to the powerful steady jet of A0620-00, while the continuum-fitting method would suggest (for a Kerr metric) that this is a slow-rotating object. If astrophysical BH candidates were objects more prolate than Kerr BHs, their spin parameter would be lower than the one reported in Table 1. In particular, for a sufficiently large deformation parameter, A0620-00 can be consistent with a fast-rotating object with a retrograde accretion disk. In this case, P_{jet} could be high, and a correlation between power of steady jets and spin parameter is possible. If we neglect a possible non-spin

contribution to the power of the jet, a simple form for P_{jet} is

$$P_{\text{jet}} = \alpha |a_*|^\beta, \quad (37)$$

and therefore

$$C = \beta \log_{10} |a_*| + \alpha' \quad (38)$$

where $\alpha' = \log_{10} \alpha$ and β are the two parameters of the jet model. If we consider the JP metric with ϵ_3 a universal constant common to all the objects, we find the best fit for $\epsilon_3 = 7.5$, $\alpha' = 30.1$, and $\beta = 2.46$ (left panel in Figure 10). If we think it is physically more plausible a deformation parameter that depends on the features of the compact object, the simplest guess is likely

$$\epsilon_3 = \gamma |a_*|^2, \quad (39)$$

with γ constant. In this case, the best fit is for $\gamma = 45$, $\alpha' = 31.2$, and $\beta = 5.65$ (right panel in Figure 10). The puzzling result in Fender et al. (2010) may thus be interpreted as an indication that BH candidates are not the Kerr BHs predicted by General Relativity (Bambi 2012d).

If we instead believe that the Blandford-Znajek mechanism is responsible for the production of transient jets, as suggested in Narayan & McClintock (2012), we can constrain possible deviations from the Kerr geometry (Bambi 2012b). Now A0620-00 shows a quite weak transient jet, which is indeed what one should expect for a slow-rotating object. If we consider objects more and more prolate than Kerr BHs, eventually, on the base of the analysis of the thermal spectrum of its disk, A0620-00 should be interpreted as a fast-rotating object with a retrograde accretion disk. This would spoil the correlation between a_* and P_{jet} , as the Blandford-Znajek mechanism would predict a powerful jet for a fast-rotating object.

For the time being we do not know if steady or transient jets are powered by the spin of the compact object and therefore we cannot really use the estimate of the jet power to test the nature of BH candidates. If we believe that the Blandford-Znajek mechanism is responsible for the production of steady jets, as it is often thought, current observations would suggest that astrophysical BH candidates are not Kerr BHs. If we believe in the proposal of Narayan & McClintock (2012), in which the Blandford-Znajek mechanism is responsible for the formation of transient jets, despite this is not the usual scenario, we can put a constraint on possible deviations from the Kerr metric. The Blandford-Znajek mechanism can unlikely be responsible for the creation of both steady and transient jets, even assuming an *ad hoc* deformation parameter for each object, as A0620-00 shows a quite powerful steady jet and a weak transient jet, which would require, respectively, either a high or a low value of the spin parameter.

4. Conclusions

Today we think the final product of the gravitational collapse is a Kerr BH and we have identified several astrophysical candidates. The latter are dark objects either in X-ray binary systems or in galactic nuclei, which are too heavy and compact to be, respectively, neutron stars or clusters of neutron stars. These two classes of objects are thought to be the Kerr BHs predicted by General Relativity because there is no alternative explanation in the framework of conventional physics. However, we have only robust measurements of the masses of these objects, while there is no clear indication that the geometry of the space-time around them is really described by the Kerr metric.

The Kerr-nature of astrophysical BH candidates may be tested with future space-based gravitational wave facilities (Ryan 1995; Glampedakis & Babak 2006; Barack & Cutler 2007), with the possible discovery of a BH binary with a pulsar companion (Wex & Kopeikin 1999), or by studying the orbital motion of new stars at milliparsec distance from the super-massive BH candidate at the center of the Galaxy (Will 2008). However, all these data are not available now and it is definitively not clear and easy to predict when they will be available in the future. Recently, there have been an increasing interest in the possibility of testing the geometry of the space-time around astrophysical BH candidates by studying the properties of the electromagnetic radiation emitted by the gas in the accretion disk. These data are in most cases already available and, thanks to the significant progresses in the last ~ 5 years, people have started using these data to extract information on the space-time geometry around BH candidates.

In this paper, I review the motivations, a possible approach, and some physical phenomena to probe the space-time geometry around BH candidates and check if they are the Kerr BHs predicted by General Relativity. The continuum-fitting method and the analysis of the $K\alpha$ iron line are relatively mature techniques. They are now commonly used by astronomers to estimate the spin parameter of these objects under the assumption of the Kerr background and they can be naturally generalized to measure possible deviations from the Kerr solution. In general, there is a strong degeneracy between the spin and the deformation parameter; that is, it is not possible to measure the spin and the deformation parameter at the same time, but only some combination of them. That is particularly true in the case of the continuum-fitting method. This degeneracy can be broken (or partially solved) if we can constrain the space-time geometry around a specific object with two or more techniques. The analysis of high frequency QPOs and of the jet power are other two interesting approaches, but the associated physical phenomena are not yet well understood and therefore, at present, they cannot really be used to test the Kerr-nature of BH candidates. In the case of the high frequency QPOs, in a Kerr background there is no way to explain all the observations with

a unique scenario and find results consistent with the continuum-fitting method. While this fact might be interpreted as a possible indication of new physics, it is definitively possible that we do not have yet the correct model to describe these phenomena or that there are systematics effects not properly taken into account. In the case of the analysis of the jet power, we do not know if steady or transient jets are powered by the spin of BH candidates. The Blandford-Znajek mechanism can explain steady jets, but a correlation between spin measurement and jet power in current data would require that the space-time around BH candidates has deviation from the Kerr solution. If we believe that the Blandford-Znajek mechanism is responsible for the production of transient jets, despite this is not the usual scenario, observations would be consistent with the interpretation that BH candidates are Kerr BHs and we can put a bound on possible deviations from the Kerr geometry.

In the near future ($\lesssim 5$ years), it is also expected that we will be able to observe the direct image of the super-massive BH candidate at the center of the Galaxy with a resolution comparable to its gravitational radius (Doeleman et al. 2008). In the case of a geometrically thick and optically thin accretion disk, we will observe the BH shadow, a dark area over a bright background, whose shape depends only on the geometry of the space-time around the compact object and it can thus be used to test the Kerr BH hypothesis (Bambi & Freese 2009; Bambi & Yoshida 2010; Johannsen & Psaltis 2010; Bambi et al. 2012; Chen & Jing 2012b).

I would like to thank Zilong Li for help in the preparation of the manuscript. This work was supported by the Thousand Young Talents Program and Fudan University.

A. Circular orbits on the equatorial plane and ISCO

The line element of a generic stationary and axisymmetric space-time can be written as

$$ds^2 = g_{tt}dt^2 + 2g_{t\phi}dtd\phi + g_{rr}dr^2 + g_{zz}dz^2 + g_{\phi\phi}d\phi^2. \quad (\text{A1})$$

Since the metric is independent of the t and ϕ coordinates, we have the conserved specific energy at infinity, E , and the conserved z -component of the specific angular momentum at infinity, L_z . This fact allows to write the t - and ϕ -component of the 4-velocity of a test-particle as

$$\dot{t} = \frac{Eg_{\phi\phi} + L_zg_{t\phi}}{g_{t\phi}^2 - g_{tt}g_{\phi\phi}}, \quad \dot{\phi} = -\frac{Eg_{t\phi} + L_zg_{tt}}{g_{t\phi}^2 - g_{tt}g_{\phi\phi}}. \quad (\text{A2})$$

From the conservation of the rest-mass, $g_{\mu\nu}\dot{x}^\mu\dot{x}^\nu = -1$, we can write

$$g_{rr}\dot{r}^2 + g_{zz}\dot{z}^2 = V_{\text{eff}}(r, z), \quad (\text{A3})$$

where the effective potential V_{eff} is given by

$$V_{\text{eff}} = \frac{E^2 g_{\phi\phi} + 2EL_z g_{t\phi} + L_z^2 g_{tt}}{g_{t\phi}^2 - g_{tt} g_{\phi\phi}} - 1. \quad (\text{A4})$$

Circular orbits in the equatorial plane are located at the zeros and the turning points of the effective potential: $\dot{r} = \dot{z} = 0$, which implies $V_{\text{eff}} = 0$, and $\ddot{r} = \ddot{z} = 0$, requiring respectively $\partial_r V_{\text{eff}} = 0$ and $\partial_z V_{\text{eff}} = 0$. From these conditions, one can obtain the angular velocity, E , and L_z of the test-particle:

$$\Omega_{\pm} = \frac{d\phi}{dt} = \frac{-\partial_r g_{t\phi} \pm \sqrt{(\partial_r g_{t\phi})^2 - (\partial_r g_{tt})(\partial_r g_{\phi\phi})}}{\partial_r g_{\phi\phi}}, \quad (\text{A5})$$

$$E = -\frac{g_{tt} + g_{t\phi}\Omega}{\sqrt{-g_{tt} - 2g_{t\phi}\Omega - g_{\phi\phi}\Omega^2}}, \quad (\text{A6})$$

$$L_z = \frac{g_{t\phi} + g_{\phi\phi}\Omega}{\sqrt{-g_{tt} - 2g_{t\phi}\Omega - g_{\phi\phi}\Omega^2}}, \quad (\text{A7})$$

where the sign $+$ is for corotating orbits and the sign $-$ for counterrotating ones. The orbits are stable under small perturbations if $\partial_r^2 V_{\text{eff}} \leq 0$ and $\partial_z^2 V_{\text{eff}} \leq 0$. In Kerr spacetime, the second condition is always satisfied, so one can deduce the radius of the ISCO from $\partial_r^2 V_{\text{eff}} = 0$. In general, however, one has to check also the stability along the vertical direction, as well as that the plunging region connects the ISCO to the surface/horizon of the compact object (Bambi & Barausse 2011b).

The radial and vertical epicyclic frequencies can be quickly computed by considering small perturbations around circular equatorial orbits, respectively along the radial and vertical direction. If δ_r and δ_θ are the small displacements around the mean orbit (i.e. $r = r_0 + \delta_r$ and $\theta = \pi/2 + \delta_\theta$), we find they are governed by the following differential equations

$$\frac{d^2 \delta_r}{dt^2} + \Omega_r^2 \delta_r = 0, \quad (\text{A8})$$

$$\frac{d^2 \delta_\theta}{dt^2} + \Omega_\theta^2 \delta_\theta = 0, \quad (\text{A9})$$

where

$$\Omega_r^2 = -\frac{1}{2g_{rr}t^2} \frac{\partial^2 V_{\text{eff}}}{\partial r^2}, \quad (\text{A10})$$

$$\Omega_\theta^2 = -\frac{1}{2g_{\theta\theta}t^2} \frac{\partial^2 V_{\text{eff}}}{\partial \theta^2}. \quad (\text{A11})$$

The radial epicyclic frequency is $\nu_r = \Omega_r/2\pi$ and the vertical epicyclic frequency is $\nu_\theta = \Omega_\theta/2\pi$.

REFERENCES

- Abramowicz, M. A., Karas, V., Kluzniak, W., Lee, W. H., & Rebusco, P. 2003 *Publ. Astron. Soc. Jap.* 55, 467
- Abramowicz, M. A., & Kluzniak, W. 2001, *A&A*374, L19
- Abramowicz, M. A., Kluzniak, W., & Lasota, J.-P. 2002, *A&A*, 396, L31
- Afshordi, N., & Paczyński, B. 2003, *ApJ*, 592, 354
- Aliev, A. N., Daylan Esmer, G., & Talazan, P. 2012, arXiv:1205.2838
- Bambi, C. 2011a, *Europhysics Letters*, 94, 50002
- Bambi, C. 2011b, *Phys. Rev. D*, 83, 103003
- Bambi, C. 2011c, *J. Cosmology Astropart. Phys.*, 5, 9
- Bambi, C. 2011d, *Modern Physics Letters A*, 26, 2453
- Bambi, C. 2011e, *Physics Letters B*, 705, 5
- Bambi, C. 2012a, *Phys. Rev. D*, 85, 043001
- Bambi, C. 2012b, *Phys. Rev. D*, 85, 043002
- Bambi, C. 2012c, *J. Cosmology Astropart. Phys.*, 9, 14
- Bambi, C. 2012d, *Phys. Rev. D*, 86, 123013
- Bambi, C. 2012e, arXiv:1205.4640
- Bambi, C. 2012f, *ApJ*, 761, 174
- Bambi, C. 2013, *Phys. Rev. D*, 87, 023007
- Bambi, C., & Barausse, E. 2011a, *ApJ*, 731, 121
- Bambi, C., & Barausse, E. 2011b, *Phys. Rev. D*, 84, 084034
- Bambi, C., Caravelli, F., & Modesto, L. 2012, *Physics Letters B*, 711, 10
- Bambi, C., & Freese, K. 2009, *Phys. Rev. D*, 79, 043002
- Bambi, C., Guainazzi, M., & Svoboda, J. 2013, in preparation

- Bambi, C., & Modesto, L. 2011, *Physics Letters B*, 706, 13
- Bambi, C., & Yoshida, N. 2010, *Classical and Quantum Gravity*, 27, 205006
- Barack, L., & Cutler, C. 2007, *Phys. Rev. D*, 75, 042003
- Barausse, E., Cardoso, V., & Khanna, G. 2010, *Physical Review Letters*, 105, 261102
- Barausse, E., Cardoso, V., & Khanna, G. 2011, *Phys. Rev. D*, 84, 104006
- Barausse, E., & Sotiriou, T. P. 2008, *Physical Review Letters*, 101, 099001
- Bardeen, J. M. 1970, *Nature*, 226, 64
- Bardeen, J. M., & Petterson, J. A. 1975, *ApJ*, 195, L65
- Bertotti, B., Iess, L., & Tortora, P. 2003, *Nature*, 425, 374
- Blandford, R. D., & Znajek, R. L. 1977, *MNRAS*, 179, 433
- Broderick, A. E., Loeb, A., & Narayan, R. 2009, *ApJ*, 701, 1357
- Carter, B. 1971, *Physical Review Letters*, 26, 331
- Chen, S., & Jing, J. 2012a, *Physics Letters B*, 711, 81
- Chen, S., & Jing, J. 2012b, *Phys. Rev. D*, 85, 124029
- Davis, S. W., Done, C., & Blaes, O. M. 2006, *ApJ*, 647, 525
- Davis, S. W., & Laor, A. 2011, *ApJ*, 728, 98
- Doeleman, S. S., Weintroub, J., Rogers, A. E. E., et al. 2008, *Nature*, 455, 78
- Dotti, G., Gleiser, R. J., Ranea-Sandoval, I. F., & Vucetich, H. 2008, *Classical and Quantum Gravity*, 25, 245012
- Elvis, M., Risaliti, G., & Zamorani, G. 2002, *ApJ*, 565, L75
- Everitt, C. W. F., Debra, D. B., Parkinson, B. W., et al. 2011, *Physical Review Letters*, 106, 221101
- Fabian, A. C., Rees, M. J., Stella, L., & White, N. E. 1989, *MNRAS*, 238, 729
- Fender, R. P., Belloni, T. M., & Gallo, E. 2004, *MNRAS*, 355, 1105
- Fender, R. P., Gallo, E., & Russell, D. 2010, *MNRAS*, 406, 1425

- Fragos, T., Tremmel, M., Rantsiou, E., & Belczynski, K. 2010, *ApJ*, 719, L79
- Giacomazzo, B., Rezzolla, L., & Stergioulas, N. 2011, *Phys. Rev. D*, 84, 024022
- Glampedakis, K., & Babak, S. 2006, *Classical and Quantum Gravity*, 23, 4167
- Gou, L., McClintock, J. E., Liu, J., et al. 2009, *ApJ*, 701, 1076
- Gou, L., McClintock, J. E., Reid, M. J., et al. 2011, *ApJ*, 742, 85
- Gou, L., McClintock, J. E., Steiner, J. F., et al. 2010, *ApJ*, 718, L122
- Hansen, R. O. 1974, *Journal of Mathematical Physics*, 15, 46
- Johannsen, T., & Psaltis, D. 2010, *ApJ*, 718, 446
- Johannsen, T., & Psaltis, D. 2011a, *ApJ*, 726, 11
- Johannsen, T., & Psaltis, D. 2011b, *Phys. Rev. D*, 83, 124015
- Johannsen, T., & Psaltis, D. 2012, arXiv:1202.6069
- Joshi, P. S., & Malafarina, D. 2011a, *International Journal of Modern Physics D*, 20, 2641
- Joshi, P. S., & Malafarina, D. 2011b, *Phys. Rev. D*, 83, 024009
- Kalogera, V., & Baym, G. 1996, *ApJ*, 470, L61
- Kato, S. 2001, *Publ. Astron. Soc. Jap.*, 53, 1
- Kluzniak, W., & Abramowicz, M. A. 2005, *Astrophys. Space Science*, 300, 143
- Kramer, M., Stairs, I. H., Manchester, R. N., et al. 2006, *Science*, 314, 97
- Li, Z., & Bambi, C. 2012, arXiv:1212.5848
- Li, L.-X., Zimmerman, E. R., Narayan, R., & McClintock, J. E. 2005, *ApJS*, 157, 335
- Liu, J., McClintock, J. E., Narayan, R., Davis, S. W., & Orosz, J. A. 2008, *ApJ*, 679, L37
- Liu, J., McClintock, J. E., Narayan, R., Davis, S. W., & Orosz, J. A. 2010, *ApJ*, 719, L109
- Lyutikov, M., & McKinney, J. C. 2011, *Phys. Rev. D*, 84, 084019
- Maoz, E. 1998, *ApJ*, 494, L181
- Martocchia, A., Karas, V., & Matt, G. 2000, *MNRAS*, 312, 817

- McClintock, J. E., Narayan, R., Davis, S. W., et al. 2011, *Classical and Quantum Gravity*, 28, 114009
- McClintock, J. E., Narayan, R., & Rybicki, G. B. 2004, *ApJ*, 615, 402
- McClintock, J. E., Shafee, R., Narayan, R., et al. 2006, *ApJ*, 652, 518
- McKinney, J. C. 2005, *ApJ*, 630, L5
- Miller, J. M. 2007 *ARA&A*, 45, 441
- Narayan, R. 2005, *New Journal of Physics*, 7, 199
- Narayan, R., & Heyl, J. S. 2002, *ApJ*, 574, L139
- Narayan, R., & McClintock, J. E. 2008, *New A Rev.*, 51, 733
- Narayan, R., & McClintock, J. E. 2012, *MNRAS*, 419, L69
- Noble, S. C., & Krolik, J. H. 2009, *ApJ*, 703, 964
- Noble, S. C., Krolik, J. H., & Hawley, J. F. 2010, *ApJ*, 711, 959
- Novikov, I. D., & Thorne, K. S. 1973, in *Black Holes*, edited by C. De Witt and B. De Witt (Gordon and Breach, New York, US), 343
- Page, D. N., & Thorne, K. S. 1974, *ApJ*, 191, 499
- Pani, P., Barausse, E., Berti, E., & Cardoso, V. 2010, *Phys. Rev. D*, 82, 044009
- Penna, R. F., McKinney, J. C., Narayan, R., et al. 2010, *MNRAS*, 408, 752
- Penna, R. F., Sä Dowski, A., & McKinney, J. C. 2012, *MNRAS*, 420, 684
- Penrose, R. 1969, *Nuovo Cimento Rivista Serie*, 1, 252
- Perez, C. A., Silbergleit, A. S., Wagoner, R. V., & Lehr, D. E. 1997, *ApJ*, 476, 589
- Price, R. H. 1972a, *Phys. Rev. D*, 5, 2419
- Price, R. H. 1972b, *Phys. Rev. D*, 5, 2439
- Psaltis, D., & Johannsen, T. 2012, *ApJ*, 745, 1
- Psaltis, D., Perrodin, D., Dienes, K. R., & Mocioiu, I. 2008, *Physical Review Letters*, 100, 091101

- Remillard, R. A., & McClintock, J. E. 2006, *ARA&A*, 44, 49
- Remillard, R. A., Muno, M. P., McClintock, J. E., & Orosz, J. A. 2002, *ApJ*, 580, 1030
- Reynolds, C. S., & Nowak, M. A. 2003, *Phys. Rep.*, 377, 389
- Rezzolla, L., Yoshida, S., Maccarone, T. J., & Zanotti, O. 2003a, *MNRAS*, 344, L37
- Rezzolla, L., Yoshida, S., & Zanotti, O. 2003b, *MNRAS*, 344, 978
- Rhoades, C. E., & Ruffini, R. 1974, *Physical Review Letters*, 32, 324
- Robinson, D. C. 1975, *Physical Review Letters*, 34, 905
- Ryan, F. D. 1995, *Phys. Rev. D*, 52, 5707
- Schnittman, J. D., & Rezzolla, L. 2006, *ApJ*, 637, L113
- Shafee, R., McClintock, J. E., Narayan, R., et al. 2006, *ApJ*, 636, L113
- Shakura, N. I., & Sunyaev, R. A. 1973, *A&A*, 24, 337
- Silbergleit, A. S., Wagoner, R. V., & Ortega-Rodríguez, M. 2001, *ApJ*, 548, 335
- Soltan, A. 1982, *MNRAS*, 200, 115
- Steiner, J. F., Reis, R. C., McClintock, J. E., et al. 2011, *MNRAS*, 416, 941
- Stella, L., & Vietri, M. 1998, *ApJ*, 492, L59
- Stella, L., & Vietri, M. 1999, *Physical Review Letters*, 82, 17
- Strohmayer, T. E. 2001, *ApJ*, 552, L49
- Tanaka, Y., Nandra, K., Fabian, A. C., et al. 1995, *Nature*, 375, 659
- Tchekhovskoy, A., Narayan, R., & McKinney, J. C. 2010, *ApJ*, 711, 50
- Tchekhovskoy, A., Narayan, R., & McKinney, J. C. 2011, *MNRAS*, 418, L79
- Titarchuk, L., Laurent, P., & Shaposhnikov, N. 2009, *ApJ*, 700, 1831
- Török, G., Abramowicz, M. A., Kluźniak, W., & Stuchlík, Z. 2005, *A&A*, 436, 1
- Török, G., Kotrlová, A., Šrámková, E., & Stuchlík, Z. 2011, *A&A*, 531, A59
- Turner, T. J., Miller, L., Reeves, J. N., & Kraemer, S. B. 2007, *A&A*, 475, 121

- Wagoner, R. V., Silbergleit, A. S., & Ortega-Rodriguez, M. 2001, *ApJ*, 559, L25
- Wang, J.-M., Chen, Y.-M., Ho, L. C., & McLure, R. J. 2006, *ApJ*, 642, L111
- Weisberg, J. M., & Taylor, J. H. 2005, *ASP Conf. Ser.*, 328, 25
- Wex, N., & Kopeikin, S. M. 1999, *ApJ*, 514, 388
- Will, C. M. 2006, *Living Reviews in Relativity*, 9, 3
- Will, C. M. 2008, *ApJ*, 674, L25
- Williams, J. G., Turyshev, S. G., & Boggs, D. H. 2004, *Physical Review Letters*, 93, 261101
- Yuan, F., Lin, J., Wu, K., & Ho, L. C. 2009, *MNRAS*, 395, 2183
- Zhang, S. N., Cui, W., & Chen, W. 1997, *ApJ*, 482, L155

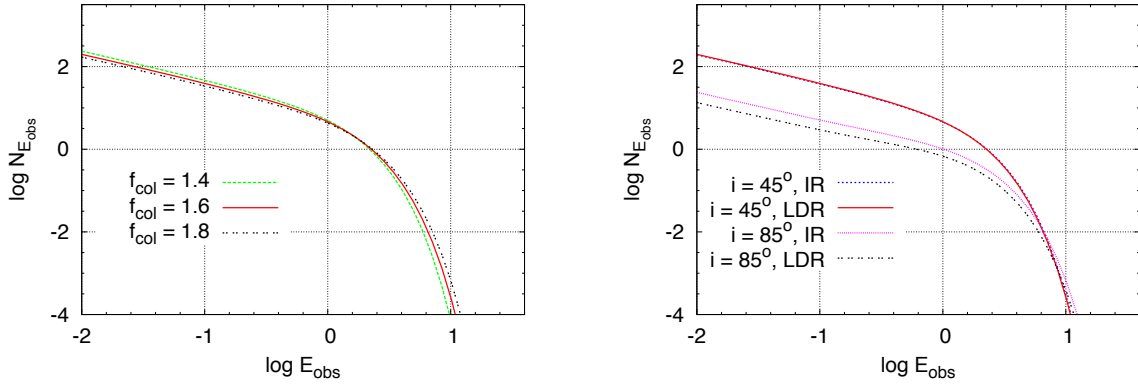


Fig. 3.— Left panel: effect of the color factor f_{col} on the thermal spectrum of a thin disk for $i = 45^\circ$. Right panel: effect of Υ on the thermal spectrum of a thin disk for $i = 45^\circ$ and 85° ; IR/LDR = isotropic/limb-darkened radiation (for $i = 45^\circ$, the two spectra are almost indistinguishable). For both panels, the parameters of the model are: $M = 10 M_\odot$, $d = 10$ kpc, $\dot{M} = 2 \cdot 10^{18} \text{ g s}^{-1}$, $a_* = 0.7$, $\epsilon_3 = 0.0$. Flux density $N_{E_{\text{obs}}}$ in $\gamma \text{ keV}^{-1} \text{ cm}^{-2} \text{ s}^{-1}$; photon energy E_{obs} in keV.

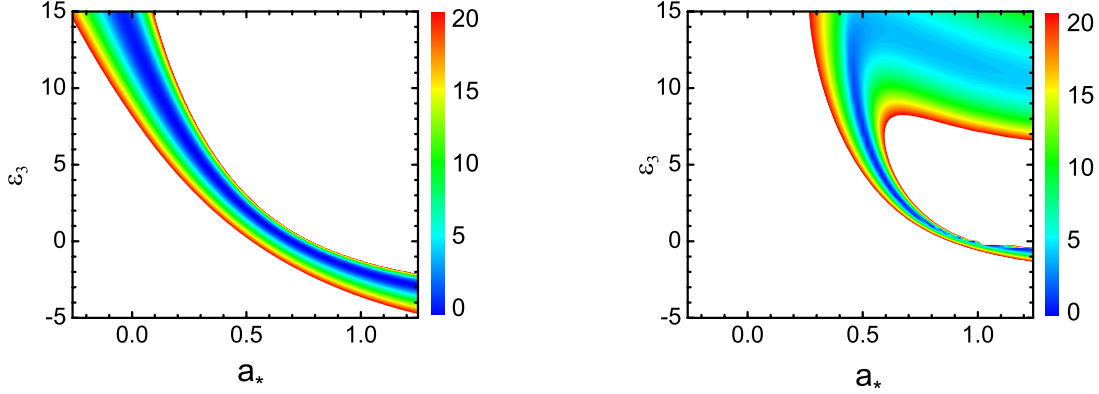


Fig. 4.— χ_{red}^2 from the comparison of the thermal spectrum of a thin accretion disk around a Kerr BH with spin parameter \tilde{a}_* and a JP BH with spin parameter a_* and deformation parameter ϵ_3 . Left panel: $\tilde{a}_* = 0.7$. Right panel: $\tilde{a}_* = 0.98$. See text for details.

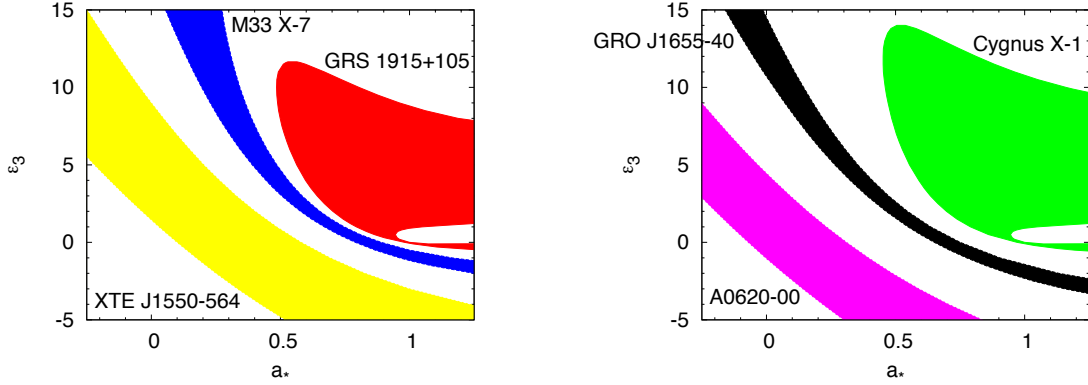


Fig. 5.— Constraints on the spin parameter-deformation parameter plane for the BH candidates GRS 1915+105 (left panel, red area), M33 X-7 (left panel, blue area), XTE J1550-564 (left panel, yellow area), Cygnus X-1 (right panel, green area), GRO J1655-40 (right panel, black area), A0620-00 (right panel, magenta area). See text for details.

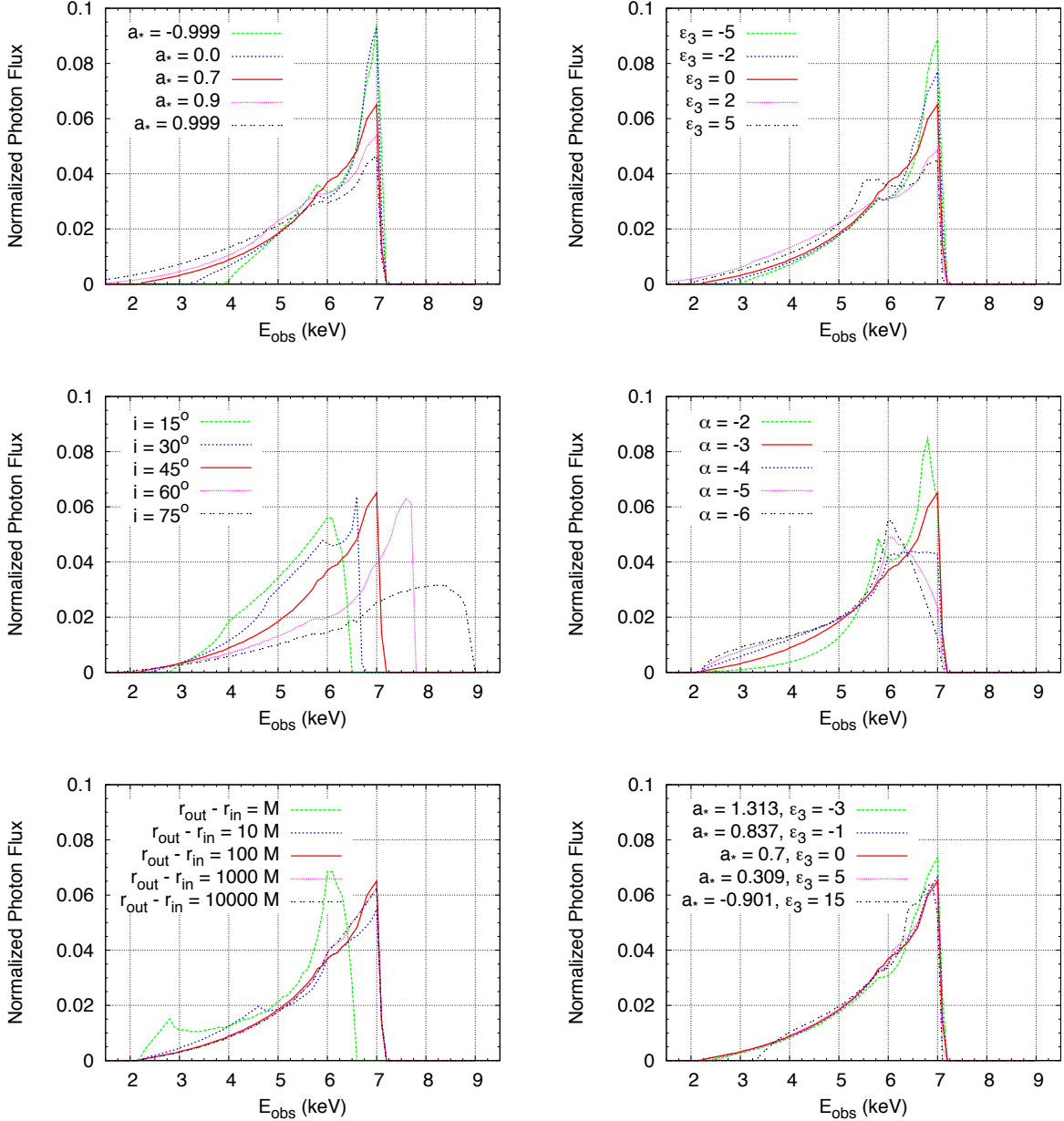


Fig. 6.— Broad $K\alpha$ iron line as a function of the parameters of the model. Left top panel: spin parameter of the BH candidate. Right top panel: deformation parameter ϵ_3 . Left central panel: disk's inclination angle with respect to the line of sight of the distant observer. Right central panel: power-law index of the intensity profile. Left bottom panel: size of the emission region. Right bottom panel: spin parameter and deformation parameter for BH candidates with the same radiative efficiency $\eta = 0.1036$. When not specified, the value of the parameters is: $a_* = 0.7$, $\epsilon_3 = 0.0$, $i = 45^\circ$, $\alpha = -3$, $r_{\text{out}} - r_{\text{in}} = 100 M$.

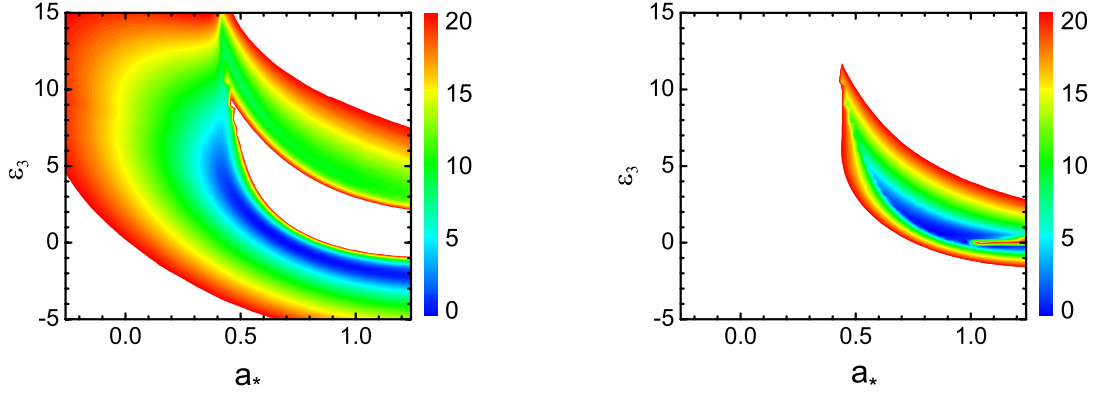


Fig. 7.— χ_{red}^2 from the comparison of the broad $\text{K}\alpha$ iron line generated around a Kerr BH with spin parameter \tilde{a}_* and a JP BH with spin parameter a_* and deformation parameter ϵ_3 . Left panel: $\tilde{a}_* = 0.7$. Right panel: $\tilde{a}_* = 0.98$. See text for details.

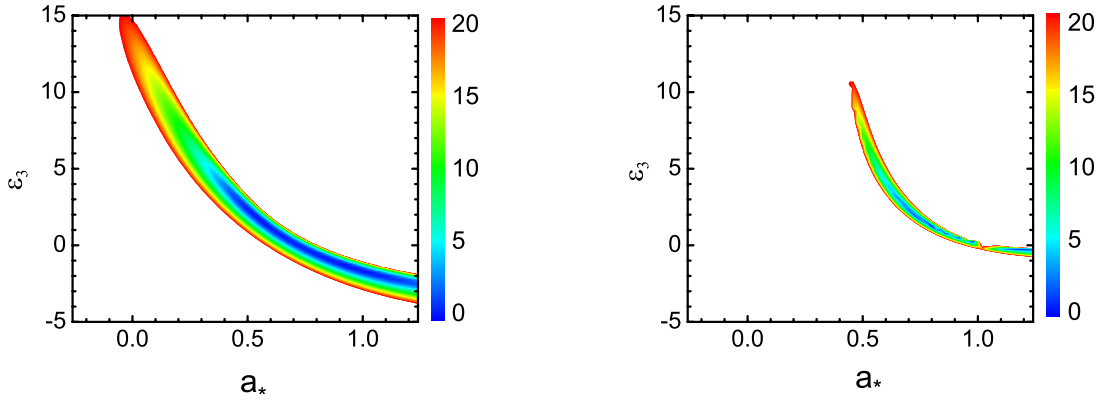


Fig. 8.— $\chi_{\text{red,tot}}^2$ from the combination of the analysis of the broad $\text{K}\alpha$ iron line and the continuum-fitting method for the case $\tilde{a}_* = 0.7$ (left panel) and $\tilde{a}_* = 0.98$ (right panel). See text for details.

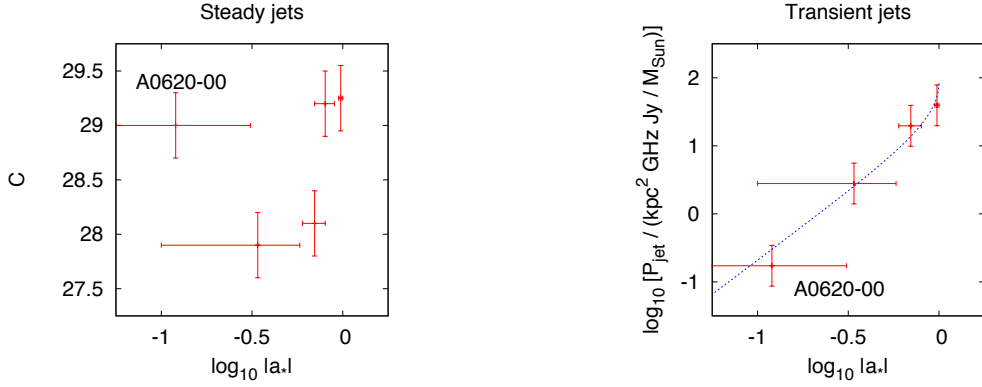


Fig. 9.— Left panel: absence of evidence for a correlation between the jet power and the BH spin for steady jets (Fender et al. 2010). Right panel: evidence for a correlation between the jet power and the BH spin for transient jets (Narayan & McClintock 2012). See text for details.

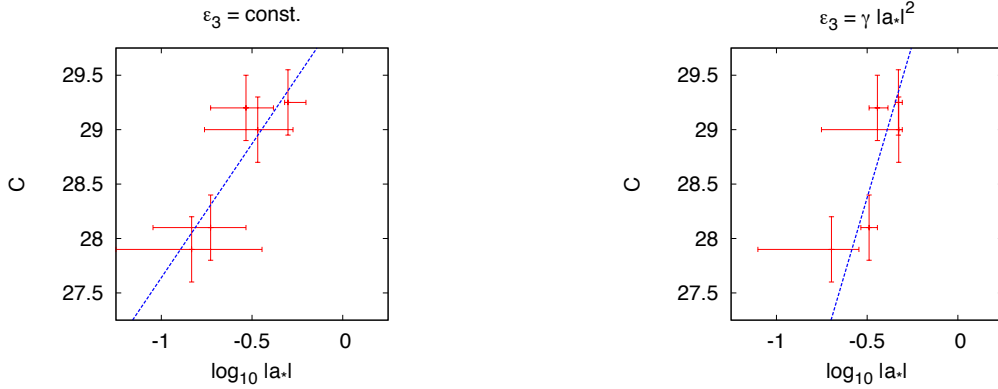


Fig. 10.— Best fit for a possible correlation between the jet power and the spin parameter of BH candidates assuming a non-vanishing deformation parameter ϵ_3 . Left panel: ϵ_3 constant for all the objects; the best fit is for $\epsilon_3 = 7.5$. Right panel: $\epsilon_3 = \gamma |a_*|^2$, with γ constant; the best fit is for $\gamma = 45$. See Bambi (2012d) for more details.